Materials Research Letters

ISSN: 2166-3831 (Online) Journal homepage: www.tandfonline.com/journals/tmrl20

Metastability-assisted fatigue behavior in a friction stir processed dual-phase high entropy alloy

K. Liu, S. S. Nene, M. Frank, S. Sinha & R. S. Mishra

To cite this article: K. Liu, S. S. Nene, M. Frank, S. Sinha & R. S. Mishra (2018) Metastability-assisted fatigue behavior in a friction stir processed dual-phase high entropy alloy, Materials Research Letters, 6:11, 613-619, DOI: 10.1080/21663831.2018.1523240

To link to this article: https://doi.org/10.1080/21663831.2018.1523240

Published online: 23 Sep 2018.

MATER. RES. LETT.
2018, VOL. 6, NO. 11, 613–619
https://doi.org/10.1080/21663831.2018.1523240

MATERIALS RESEARCH LETTERS
Taylor & Francis
Taylor & Francis Group

ORIGINAL REPORTS

Metastability-assisted fatigue behavior in a friction stir processed dual-phase high entropy alloy

K. Liu, S. S. Nene, M. Frank, S. Sinha and R. S. Mishra

Center for Friction Stir Processing, Department of Materials Science and Engineering, University of North Texas, Denton, TX, USA

ABSTRACT

Metastability-based high entropy alloy design opens a new strategic path for designing high-strength materials. However, high strength is always coupled with poor damage tolerance under cyclic loading conditions (fatigue). To overcome this drawback, here we present grain-refined $Fe_{42}Mn_{28}Cr_{15}Co_{10}Si_5$ exhibiting significantly high fatigue strength as compared with leading transformation induced plasticity steels upon friction stir processing. The enhanced fatigue behavior is attributed to the metastability-promoted $\gamma \rightarrow \varepsilon$ transformation that caused local variation in work-hardening activity near the crack tip, and subsequent crack branching. Thus, decreased γ phase stability assisted not only in attaining strength but also in making the alloy fatigue-resistant.

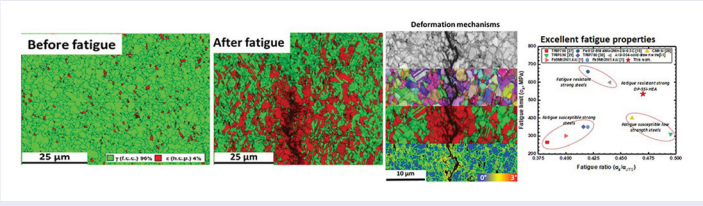

ARTICLE HISTORY
Received 7 July 2018

KEYWORDS
Metastability; fatigue limit; TRIP; high entropy alloy

IMPACT STATEMENT

Fatigue resistance of dual-phase TRIP $Fe_{42}Mn_{28}Cr_{15}Co_{10}Si_5$ was evaluated. Metastability-promoted $\gamma \rightarrow \varepsilon$ transformation improved fatigue life due to local enhancement in work-hardening near the crack tip.

Introduction

Fatigue behavior of materials is influenced by microstructural, environmental, and geometrical factors. In terms of the microstructure, superior fatigue crack resistance can be obtained by various micromechanisms that resist crack propagation. Hence, tuning these micromechanisms during deformation is critical to altering the fatigue response of the material. Aligned with this, Koyama et al. [1] attained a bone-like microstructure having nano-laminated arrangements of metastable phases. They further claimed that a bone-like structure assisted in arresting cracks and ultimately improved fatigue property. Formation of deformation twins or ε martensite plates could also alter the crack growth path during cyclic loading because of localized variation in work hardening activity [2–4]. In this context, Cheng et al. [2] reported that intense local plasticity arises due to transformation, which enhances work hardening; and, consequently, uniform strain is increased significantly at the crack tip. As a result, localized strain hardening activity forms a necking zone at the crack tip, thereby ensuring excellent tear resistance. Earlier work on fatigue behavior of transformation induced plasticity (TRIP) steels suggested that damage starts to accumulate only after austenite has transformed into martensite, whereby the void nucleation mechanism has also been affected [5]. Further, $\gamma \rightarrow \varepsilon$ transformation at the crack tip is beneficial in arresting crack growth owing to extreme strain mismatch at the γ/ε interfaces, thereby causing a local work hardening phenomenon [6–18]. Our recent work on dual phase $Fe_{50}Mn_{30}Cr_{10}Co_{10}$ (at. %) (DP-HEA) confirmed significant tensile property enhancement by grain size refinement through FSP [4]. After FSP, DP-HEA showed an average grain size of $\sim 5.2\,\mu$m and exhibited

CONTACT R. S. Mishra Rajiv.Mishra@unt.edu Center for Friction Stir Processing, Department of Materials Science and Engineering, University of North Texas, Denton, TX 76203, USA

a yield strength (YS) of 400 MPa [4]. Further, the addition of Si in $Fe_{42}Mn_{28}Cr_{15}Co_{10}Si_5$ (DP-5Si-HEA) altered the γ phase stability and assisted in grain refinement during FSP (to an average grain size of $\sim 1.97\,\mu$m from as–cast grain average grain size of $\sim 100\,\mu$m). As a result, YS of DP-5Si-HEA was observed to be exceptionally high (950 MPa) with an ultimate tensile strength (UTS) of 1.15 GPa [19]. These enhanced mechanical properties were attributed to the exceptional work hardening ability of the material through controlled transformation and twinning-assisted deformation [19]. Adaptive deformation accommodation is a result of extreme metastability of the γ matrix attained by adding Si [19]. Hence, whether the flexible microstructural evolution that resulted from metastability-based phase stability in DP-5Si-HEA is beneficial for improving fatigue crack resistance is indeed worth exploring.

Thus, the present work is focused on examining fatigue behavior of the metastable DP-5Si-HEA under constant stress cycles. As reported in our recent work [19], multi-pass FSP on the same HEA system showed very high YS and near ultrafine microstructure. Stress-controlled, fully reversible bending fatigue tests were performed for the same processing condition. Additionally, the effect of transformation of metastable γ matrix on crack growth is presented with the assistance of interrupted fatigue tests.

Experimental

The DP-5Si-HEA was produced using a vacuum induction furnace backfilled with argon to 1 atm in a cold copper crucible, with a nominal composition of $Fe_{42}Mn_{28}Cr_{15}Co_{10}Si_5$ (at. %). The dimensions of the final cast material was 250 mm × 80 mm × 5 mm. The as-cast material with 5 mm starting thickness was severely deformed by multi-pass FSP using the parameters shown in Table 1. The processing tool had a tapered pin with shoulder, root, and distal tip diameters of 12, 7.5, and 6 mm, respectively. The pin length was 3.5 mm.

Back-scattered electron microscopy (BSE) and energy-dispersive X-ray spectroscopy (EDS) were carried out using FEI Nova NanoSEM230. Grain size and distribution and phase fraction were obtained using orientation imaging microscopy (OIM) on FEI Nova NanoSEM230, with 20 kV accelerating voltage and 6.1 nA probe current. X-ray diffraction (XRD) measurements were performed using RIGAKU X-Ray equipment, with Cu K_α radiation operated at 40 kV and 30 mA. 1 mm thick mini tensile samples were obtained from the nugget region 1 mm below the processed top surface. Mini tensile and fatigue samples were machined using a computer numerical control machine. The tensile samples with gage length ~ 5 mm, width ~ 1.2 mm, and thickness ~ 1.1 mm were tested using a computer-controlled mini-tensile machine at an initial strain rate of $10^{-3}\,s^{-1}$. Fully reversed ($R = -1$) bending fatigue tests were performed with a custom-made tabletop fatigue testing machine at 20 Hz. Sample dimensions and machine details are given in [3]. Tensile and fatigue samples were polished with SiC papers to 1200 grit, and final polishing with 1 μm diamond suspension. Fatigue and microscopy samples were further polished with 0.05 and 0.02 μm colloidal silica suspensions.

Table 1. Processing parameters selected for FSP.

Processing parameters	Pass 1	Pass 2	Pass 3
Rotational Rate (RPM)	650	350	250
Traverse Speed (mm/min)	50.8	50.8	50.8
Plunge Depth (mm)	3.85	3.85	3.85
Tilt Angle (°)	2.0	2.0	2.0

Figure 1(a) shows an electron backscatter diffraction (EBSD) inverse pole figure (IPF) map for the nugget region after FSP, where a fully recrystallized microstructure with an average grain size of $1.97 \pm 1.03\,\mu$m was obtained by multi-pass FSP. Multiple passes promote not only chemical homogeneity but also adaptive phase stability [4,19] while the consecutive decrease in tool rotation rate leads to severe refinement of grains leading to homogenous very fine grained microstructure. Accordingly, multi-pass of DP-5 Si-HEA resulted in very fine grained microstructure with almost $\sim$96% f.c.c. γ and $\sim$4% h.c.p. ε phases (Figure 1(b)). The phase fraction was confirmed by XRD analysis (Figure 1(c)), and the diffraction peaks suggested that f.c.c. γ has become the dominant phase in the nugget region after FSP. FSP led to a higher fraction of the f.c.c. γ phase in the microstructure of the TRIP HEA irrespective of tool rotational rates. Phase evolution in DP-5Si-HEA is discussed in detail in [19]. Figure 1(d) presents the distribution of grain size in the nugget region, where a recrystallized homogeneous microstructure was observed [20]. The resultant microstructure from FSP showed a higher work hardening rate over an extended plastic strain range due to TRIP [4].

Tensile strength of the FSP nugget was investigated through tensile testing, as the tensile property of an alloy is closely related to its fatigue behavior. Figure 2(a) shows the engineering stress–strain response for the FSPed sample. FSP resulted in the YS of $\sim$957 MPa and the UTS of $\sim$1158 MPa, with a total elongation of $\sim$15%. Enhanced tensile strength is attributed to the resultant phase evolution in the microstructure after FSP, as well as to refinement of the grain size in the nugget region. In addition to FSP, Si is a grain refiner due to its smallest atomic radius

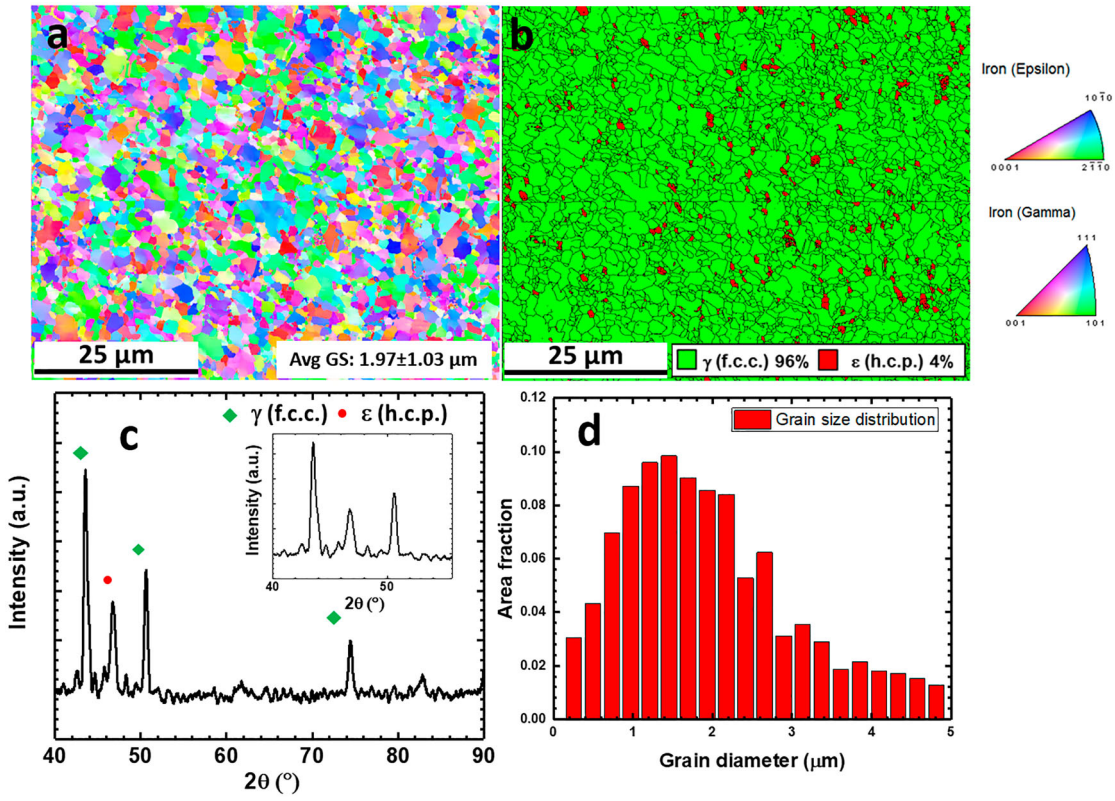

Figure 1. Initial microstructure after FSP, (a) inverse pole figure map in the multi-pass nugget region, (b) phase map in the multi-pass nugget region with high angle grain boundaries highlighted by black lines, (c) XRD pattern at the nugget region, and (d) grain size distribution in the nugget region.

among all other elements contained in the alloy. Dislocation storage was enhanced due to the higher grain boundary area available upon severe grain refinement in the M-pass specimen just before yielding [4]. On the other hand, the newly-formed (transformation during deformation) as well as pre-existing (upon FSP) harder h.c.p. ε phases act as sites of dislocation pile-up after transformation, which consequently improved alloy work hardenability. In addition, the extremely metastable γ matrix was key to attaining such a high work hardening ability in DP-5Si-HEA [19]. Moreover, the work hardening rate plot (Figure 2(b)) suggests that the newly formed ε phase was also able to undergo twinning at later stages of deformation, and helped to obtain reasonable elongation in the alloy even at higher YS.

In addition to tensile properties, fatigue properties also are important to the integrity of structural materials, as most of the structural components undergo cyclic loading while in service, and fatigue is a major cause of failure of structural components [22]. Figure 2(c) shows the S-N curve obtained from a fully reversible bending fatigue test, where the DP-5Si-HEA depicted exceptional fatigue property. Under the fully reversible cyclic stress of $\sim$800 MPa, the material remained in the high cycle fatigue (HCF) regime. The fatigue behavior of this alloy is well-maintained as compared to other available HEA fatigue results and is due mainly to rapid $\gamma \rightarrow \varepsilon$ transformation. The number of cycles to failure increases with decrease in fatigue stress amplitude as expected. Moreover, the fatigue ratio (fatigue run-out stress amplitude/UTS) is greater than 0.46 UTS, with a run-out stress amplitude greater than 535 MPa. As compared to most other commercially available TRIP steels [24–26], dual phase steels and TRIP-DP steels, the fatigue run-out is superior (Figure 2(d)).

Fractography was done to examine the fatigue failure features at the fracture surfaces for specimens tested at different stress amplitudes (Figure 2(e_1, e_2)). Typical fatigue failure with three major stages was seen for specimen tested at a stress level near fatigue run-out. Referring to the fatigue crack growth theory [22], stage II of crack propagation is associated with the crack blunting process (the Paris-law regime with lower slope of crack growth rate change with the stress intensity) and hence determines the life of crack growth. In the present work, $\gamma \rightarrow \varepsilon$ transformation[21] within the crack tip plastic zone triggers localized work hardening (WH) activity which alters crack propagation drastically. Severe

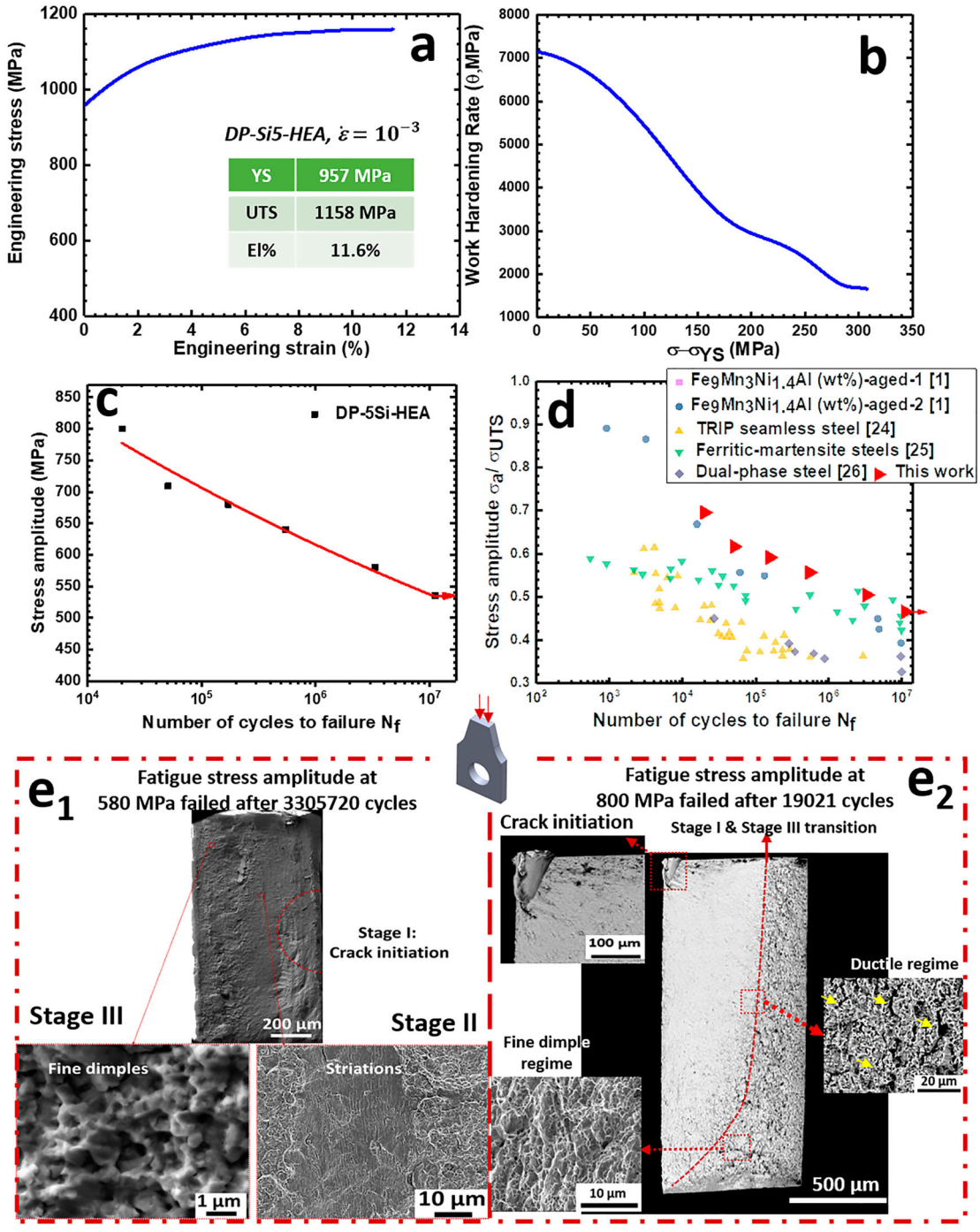

Figure 2. Tensile and fatigue behavior. (a) Engineering stress-strain curve following multi-pass FSP. (b) Work hardening rate vs. flow stress curve, (c) S-N curve for fully reversible fatigue testing. (d) Comparison of the S-N curves for current alloy with other TRIP alloys. Comparison of fractographs from (e_1) a sample tested at the cyclic stress of 580 MPa after failure at 3305720 cycles, and (e_2) a sample at the cyclic stress of 800 MPa after failure at 19021 cycles.

crack branching near the transformed region also points towards the crack blunting process which ultimately delays the crack propagation. Once the fatigue crack nucleates and grows beyond microstructurally small crack (end of stage I), stress intensity at the crack tip start dominating the crack growth. For a given crack length size, the stress intensity is proportional to the nominal applied stress, and would be higher for the 800 MPa specimen than the 580 MPa specimen. This would reduce the time for localized work hardening activity in the 800 MPa specimen, leading to marginal crack branching and hence does not show typical fatigue failure morphology. Further, it is common in two phase alloys to exhibit tire track marks at higher stress amplitude, which is observed in

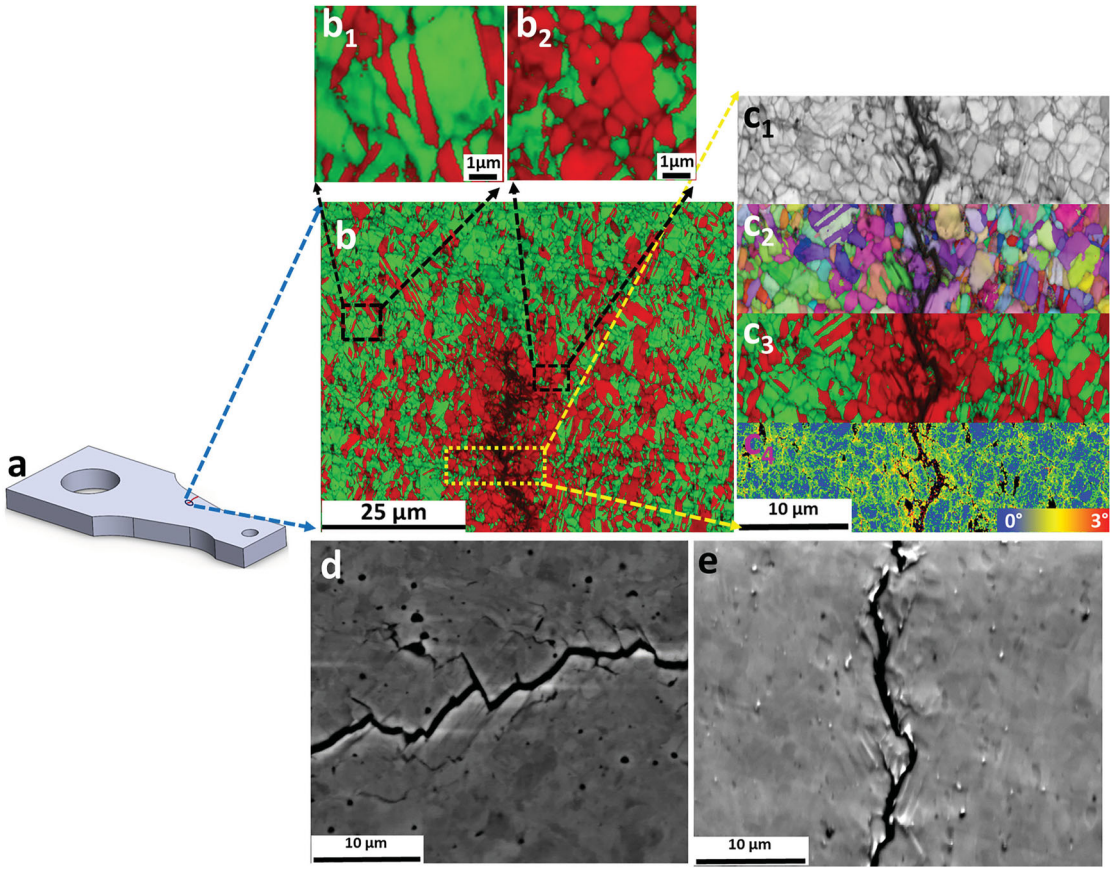

Figure 3. Microstructural characterization for interrupted fatigue test. (a) Schematic representation of scan location with respect to the actual fatigue sample. (b) Phase map at the crack tip on the fatigue sample, (c_1–c_4) higher magnification scan around the crack with image quality map, IPF map, phase map, and KAM, respectively. (d) BSE image at the crack reveals the fatigue branching cracks. (e) Pattern Region of Interest Analysis System (PRIAS) top image at the crack region reveals crack branching along the formed twin boundaries in the h.c.p. phase.

Figure 2(e_2). However, presence of very fine striations indicating existence of distinct stage II due to increased resistance to crack propagation in low stress (580 MPa) amplitude specimen. In line with the fatigue failure theory, both stress amplitude specimens showed a typical overload fracture morphology (Stage III), where typical ductile failure with very fine dimples were observed.

Exploring the fatigue behavior of the material by understanding the deformation accommodation mechanism once the crack has nucleated is important. After the crack initiates, its propagation depends on the local hardening mechanism (such as transformation or twinning). This localized hardening occurs within the plastic zone near the crack tip and promotes crack branching and delays crack growth [1]. Therefore, crack propagation is also associated with the consumption of strain energy. As the crack starts from one surface, bending stress on that surface reduces, while that of the other surface remains constant [23]. To study this in detail, the fatigue test was interrupted after 121551 cycles, corresponding to 680 MPa fully reversible cyclic stress amplitude. The interrupted sample was analyzed with EBSD to quantify the phase fraction change surrounding the cracked region. Figure 3(a) is a schematic representation of the scan location. The phase map (Figure 3(b)) of substantial color change to red from green in the plastic zone of the crack confirmed pronounced $\gamma \rightarrow \varepsilon$ transformation. Figure 3(c_1–c_4) show a high resolution scan around the crack, with its corresponding image quality, IPF, phase fraction, and Kernel average misorientation (KAM) maps, respectively. The transformation is attributed to the presence of an extremely metastable γ matrix as the starting microstructure. The increased metastability in DP-5Si-HEA is responsible for the transformation surrounding the crack tip. Crack propagation also involves plastic strain accommodation. KAM distribution near the crack tip and higher KAM values in the ε phase field point to the active involvement of ε in plastic deformation. Furthermore, the morphology of the formed h.c.p. phase is also changing away from the cracked surface. The h.c.p. plates formed away from the crack appeared to be thin; whereas closer to the crack,

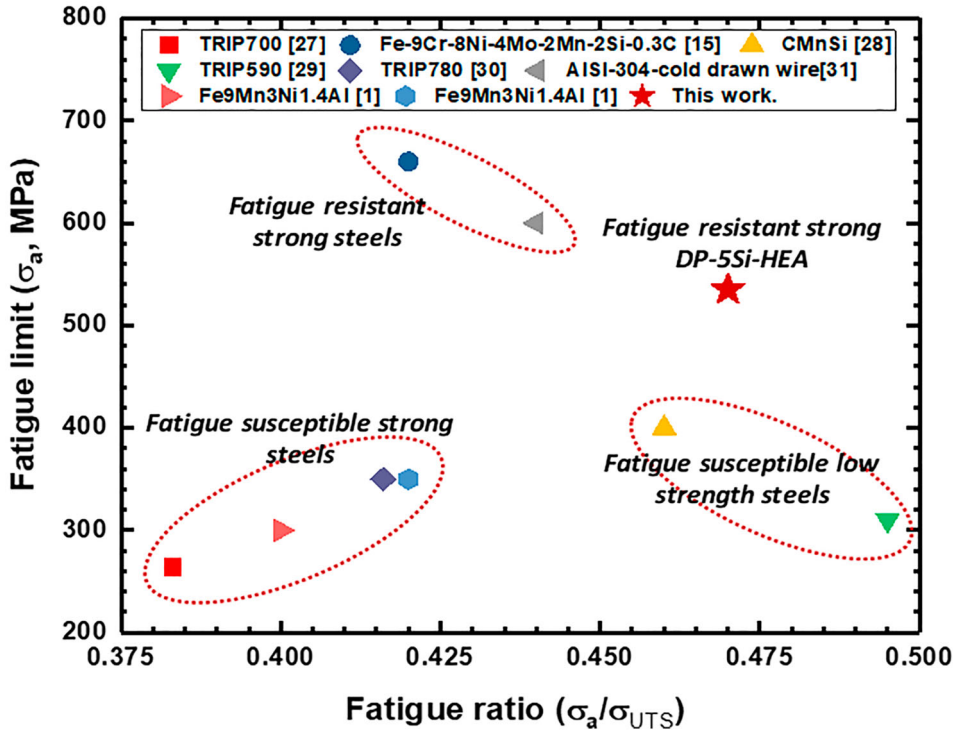

Figure 4. Fatigue limit (σ_a) vs fatigue ratio plot for a variety of TRIP steels and DP-5Si-HEA.

the plates appeared to be thicker. Lastly, the thicker plates grow to full grains near the cracked surface. This morphological evolution is also related to branching of the cracks. These micro-cracks formed along with the major crack shared the excess energy and delayed crack propagation (Figure 3(d)). Crack branching can be related directly to the pronounced transformation of the γ to the ε phase in the plastic zone that creates localized strain mismatch and undergoes work hardening via the dynamic Hall-Petch effect. Additionally, the formation of deformation twins in the ε phase is another source of energy dissipation in the plastic zone. Furthermore, the cracks branch along with the deformation twin boundaries in the epsilon phase; and persistent slip band extrusion has been observed (Figure 3(e)). In short, improved fatigue life is associated with localized work hardening in the crack plastic zone via controlled transformation and twinning effects.

Figure 4 compares fatigue limit (σ_a) and fatigue ratio for a variety of TRIP steels studied thus far [1,15,27–31]. Figure 4 confirms that DP-5Si-HEA outperforms all TRIP steels in terms of fatigue strength (535 MPa), thereby showing its strong potential for use in cyclic loading conditions. The metastable γ phase and resulting TRIP effect appear to have been crucial to attaining simultaneous improvement in both fatigue limit and UTS (1150 MPa) of the material, and ultimately led to a high fatigue ratio (0.46). This result is attributed to the abundant compositional space available for dual phase HEA. The synergistic effect of Si addition and the severe deformation imposed during multi-pass FSP towards grain refinement and γ phase stability [4,19,32] helped to obtain the near ultrafine grained microstructure that ultimately improved the fatigue response of the material.

In summary, multi-pass FSP of DP-5Si-HEA resulted in substantial grain refinement and phase redistribution throughout the nugget, thereby significantly increasing its YS and UTS. This grain-refined HEA further demonstrated unconventional fatigue response owing to extreme metastability of the γ matrix. The pronounced $\gamma \rightarrow \varepsilon$ transformation within the crack plastic zone enhanced work hardening which reduced crack growth and also promotes crack branching. The simultaneous improvement in fatigue limit and fatigue ratio in comparison with TRIP steels makes DP-5Si-HEA a strong candidate for cyclic loading applications.

Acknowledgments

Authors gratefully acknowledge the support of National Science Foundation through grant #1435810. The authors are thankful to the Center for Advanced Research and Technology for providing access to the microscopy facilities at the University of North Texas.

Disclosure statement

No potential conflict of interest was reported by the authors.

Funding

This work was supported by National Science Foundation [grant number 1435810].

ORCID

S. S. Nene http://orcid.org/0000-0002-4236-422X
R. S. Mishra http://orcid.org/0000-0002-1699-0614

References

[1] Koyama M, Zhang Z, Wang M, et al. Bone-like crack resistance in hierarchical metastable nanolaminate steels. Science. 2017;355:1055–1057.
[2] Cheng X, Petrov R, Zhao L, et al. Fatigue crack growth in TRIP steel under positive R-ratios. Eng Fract Mech. 2008;75:739–749.
[3] De P, Obermark C, Mishra R. Development of a reversible bending fatigue test bed to evaluate bulk properties using sub-size specimens. J Test Eval. 2008;36:402–405.
[4] Nene S, Liu K, Frank M, et al. Enhanced strength and ductility in a friction stir processing engineered dual phase high entropy alloy. Sci Rep. 2017;7:299.
[5] Niendorf T, Wegener T, Li Z, et al. Unexpected cyclic stress-strain response of dual-phase high-entropy alloys induced by partial reversibility of deformation. Scr Mater. 2018;143:63–67.
[6] Abareshi M, Emadoddin E. Effect of retained austenite characteristics on fatigue behavior and tensile properties of transformation induced plasticity steel. Mater Des. 2011;32:5099–5105.
[7] Niendorf T, Lotze C, Canadinc D, et al. The role of monotonic pre-deformation on the fatigue performance of a high-manganese austenitic TWIP steel. Mater Sci Eng A. 2009;499:518–524.
[8] Sugimoto K, Fiji D, Yoshikawa N. Fatigue strength of newly developed high-strength low alloy TRIP-aided steels with good hardenability. Procedia Eng. 2010;2:359–362.
[9] Cheng Xu, Petrov Roumen, Zhao Lie, et al. Fatigue crack growth in TRIP steel under positive R-ratios. Engineering Fracture Mechanics. 2008;75:739.
[10] Hu Z, Zhu P, Meng J. Fatigue properties of transformation-induced plasticity and dual-phase steels for auto-body lightweight: experiment, modeling and application. Mater Des. 2010;31:2884–2890.
[11] Olson GB, Chait R, Azrin M, et al. Fatigue strength of TRIP steels. Metall Mater Trans A. 1980;11:1069–1071.
[12] Yasuki S, Sugimoto K, Kobayashi M, et al. Low cycle fatigue-hardening of TRIP-aided dual-phase steels. I J Japan Inst Met. 1990;54:1350–1357.
[13] Huo C, Gao H. Strain-induced martensitic transformation in fatigue crack tip zone for a high strength steel. Mater Charact. 2005;55:12–18.
[14] Miranda O, Carlos A, Meggiolaro MA, et al. Fatigue life prediction of complex 2D components under mixed-mode variable amplitude loading. Int J Fatigue. 2003;25:1157–1167.
[15] Sugimouto K, Kobayashi M, Yasuki S. Cyclic deformation behavior of a transformation-induced plasticity-aided dual-phase steel. Metall Mater Trans A. 1997;28:2637–2644.
[16] Nikulin I, Sawaguchi T, Tsuzaki K. Effect of alloying composition on low-cycle fatigue properties and microstructure of Fe–30Mn–(6−x)Si–xAl TRIP/TWIP alloys. Mater Sci Eng A. 2013;587:192–200.
[17] Nikulin I, Sawaguchi T, Ogawa K, et al. Effect of γ to ε martensitic transformation on low-cycle fatigue behavior and fatigue microstructure of Fe–15Mn–10Cr–8Ni–xSi austenitic alloys. Acta Mater. 2016;105:207–218.
[18] Birol Y. What happens to the energy input during fatigue crack propagation? Mater Sci Eng A. 1988;104:117–124.
[19] Nene S, Frank M, Liu K, et al. Extremely high strength and work hardening ability in a metastable high entropy alloy. Sci Rep. 2018;8:227.
[20] Sun S, Tian Y, Lin H, et al. Enhanced strength and ductility of bulk CoCrFeMnNi high entropy alloy having fully recrystallized ultrafine-grained structure. Mater Des. 2017;133:122–127.
[21] Olson G, Cohen M. A general mechanism of martensitic nucleation: Part I. General concepts and the FCC → HCP transformation. Metallurgical Transactions A. 1976;7:1897.
[22] Suresh S. Fatigue of materials. Cambridge: Cambridge University Press; 1998.
[23] Kapoor R, Rao V, Mishra R, et al. Probabilistic fatigue life prediction model for alloys with defects: applied to A206. Acta Mater. 2011;59:3447–3462.
[24] Zhang Z, Li Y, Manabe K, et al. Effect of heat treatment on microstructure and mechanical properties of TRIP seamless steel tube. Mater Trans. 2012;53:833–837.
[25] Aran A, Türker H. The effect of martensite content on the fatigue behaviour of a ferritic-martensitic steel. J. Mater Sci Lett. 1990;9:1407–1408.
[26] Cai X, Feng J, Owen W. The dependence of some tensile and fatigue properties of a dual-phase steel on its microstructure. Metall Mater Trans A. 1985;16:1405–1415.
[27] Haidemenopoulos G, Kermanidis A, Malliaros C, et al. On the effect of austenite stability on high cycle fatigue of TRIP 700 steel. Mater Sci Eng A. 2013;573:7–11.
[28] Abareshi M, Emadoddin E. Effect of retained austenite characteristics on fatigue behavior and tensile properties of transformation induced plasticity steel. Materials & Design. 2011;32:5099.
[29] Islam M, Chen S, Tomota Y. Tensile and plane bending fatigue properties of two TRIP steels at room temperature in the air—a comparative study. J Mater Eng Perform. 2007;16:248–253.
[30] Ly L, Findley K. The effects of pre-straining conditions on fatigue behavior of a multiphase TRIP steel. Int J Fatigue. 2016;87:225–234.
[31] Fredj B, Nasr B, Rhouma B, et al. Fatigue life improvements of the AISI 304 stainless steel ground surfaces by wire brushing. J Mater Eng Perform. 2004;13:564–574.
[32] Nene S, Frank M, Liu K, et al Reversed strength-ductility relationship in microstructurally flexible high entropy alloy. Scripta Materialia. 2018;154:163.